Efficient β-Sheet Identification in Proteins by Solid-State NMR Spectroscopy

Daniel Huster, Satoru Yamaguchi, and Mei Hong*

Contribution from the Department of Chemistry, Gilman Hall 0108, Iowa State University, Ames, Iowa 50011

Received May 15, 2000. Revised Manuscript Received September 13, 2000

Abstract: An efficient two-dimensional magic-angle-spinning (MAS) NMR technique to selectively detect β-sheet residues in proteins is demonstrated. The method exploits the relative orientation between N−H and Cα−Hα dipolar couplings, that is, the ϕ torsion angle, in each amino acid residue. The different ϕ angles between the α-helical and β-sheet conformations give rise to distinctly different dipolar modulations. After one-half of a rotation period of dipolar evolution, β-sheet residues retain significant intensities (20−50%), while α-helical signals vanish for suitable spinning speeds. Thus, a distinction between sheet and helix geometries can be achieved without lengthy measurements of the entire dipolar modulation curve. Combining this constant-time dipolar modulation with 2D ^{15}N−^{13}C correlation, we selected the β-sheet signals and removed the α-helical resonances in mixtures of model amino acids *N*-acetyl valine and *N*-tBoc alanine. To demonstrate the suitability of this technique for solid proteins, β-sheet filtration was applied to ^{13}C- and ^{15}N-labeled ubiquitin. Two pulse sequences that are suitable for slow ($\sim$4 kHz) and faster spinning speeds ($\sim$7 kHz) are compared. The technique represents a complementary approach to the recently introduced α-helix filter experiment (Hong, *J. Am. Chem. Soc.* **122** (2000) 3762−3770) and is expected to further enhance the efficiency and confidence of protein structure determination by solid-state NMR.

Introduction

Structure determination of insoluble and noncrystallizable proteins remains a challenge in structural biology. In particular, the structure of membrane-bound proteins has attracted increasing interest in the post-genomic era as more membrane proteins are discovered with a diverse array of biological functions, such as cell signaling and transport.

Solid-state nuclear magnetic resonance spectroscopy (NMR) is a promising technique for elucidating the three-dimensional structure of solid proteins. Recently, a number of solid-state NMR methods have been developed to measure the ϕ and ψ torsion angles of the polypeptide backbone.[1−9] These experiments correlate dipolar and/or chemical-shift tensors of nuclear spins to extract the relative orientation between two tensors about the torsion bond of interest. Many of these experiments encode the torsion angle information in one dimension and the chemical-shift dispersion in the other. To determine the structure of large proteins efficiently, it is desirable to incorporate many isotopic labels so that multiple torsion angles can be measured in each experiment. For such extensively labeled proteins, the chemical-shift resolution available in one dimension is limited, and resonance overlap is severe.[10] This problem can, in principle, be alleviated by extending the experiment to three dimensions in which two chemical-shift dimensions separate the resonances, and the third dimension encodes the torsion angle information. However, such a three-dimensional (3D) experiment requires extensive signal averaging and, thus, has limited applicability to realistically sized proteins.[11]

A considerable gain in sensitivity may be obtained by designing these experiments as conformation selection filters. An example is a Cα chemical-shift-anisotropy filter technique that we introduced recently to identify helical residues in proteins.[12] The experiment exploits the correlation between the Cα chemical-shift anisotropy (CSA) and secondary structure: α-helical residues have smaller CSAs than β-sheet residues.[13,14] By modulating the magnetization with the recoupled CSA interaction and choosing the time point where the intensities for the helix and sheet conformations differ the most, we selected the signals of helical residues while filtering out the β-sheet signals. To resolve more resonances, we combined the CSA-filter sequence with a two-dimensional (2D) ^{15}N−^{13}C heteronuclear correlation experiment.[15−18] Applied to ubiquitin, this

* Corresponding author: Telephone: (515) 294-3521. Fax: (515) 294-0105. E-mail: mhong@iastate.edu.

(1) Schmidt-Rohr, K. *J. Am. Chem. Soc.* **1996,** *118,* 7601−7603.
(2) Weliky, D.; Tycko, R. *J. Am. Chem. Soc.* **1996,** *118,* 8487−8488.
(3) Ishii, Y.; Terao, T.; Kainosho, M. *Chem. Phys. Lett.* **1996,** *256,* 133−140.
(4) Feng, X.; Eden, M.; Brinkmann, A.; Luthman, H.; Eriksson, L.; Graslund, A.; Antzutkin, O. N.; Levitt, M. H. *J. Am. Chem. Soc.* **1997,** *119,* 12006−12007.
(5) Hong, M.; Gross, J. D.; Griffin, R. G. *J. Phys. Chem. B* **1997,** *101,* 5869−5874.
(6) Costa, P. R.; Gross, J. D.; Hong, M.; Griffin, R. G. *Chem. Phys. Lett.* **1997,** *280,* 95−103.
(7) Long, H. W.; Tycko, R. *J. Am. Chem. Soc.* **1998,** *120,* 7039−7048.
(8) Hong, M.; Gross, J. D.; Hu, W.; Griffin, R. G. *J. Magn. Reson.* **1998,** *135,* 169−177.
(9) Bower, P. V.; Oyler, N.; Mehta, M. A.; Long, J. R.; Stayton, P. S.; Drobny, G. P. *J. Am. Chem. Soc.* **1999,** *121,* 8373−8375.

(10) Hong, M. *J. Magn. Reson.* **1999,** *139,* 389−401.
(11) Rienstra, C. M.; Hohwy, M.; Mueller, L. J.; Reif, B.; Jaroniec, C. P.; Tucker-Kellogg, L.; Tidor, B.; Griffin, R. G. *41st Experimental Nuclear Magnetic Resonance Conference*; Asilomar, CA, 2000.
(12) Hong, M. *J. Am. Chem. Soc.* **2000,** *122,* 3762−3770.
(13) Tjandra, N.; Bax, A. *J. Am. Chem. Soc.* **1997,** *119,* 9576−9577.
(14) Havlin, R. H.; Le, H.; Laws, D. D.; deDios, A. C.; Oldfield, E. *J. Am. Chem. Soc.* **1997,** *119,* 11951−11958.
(15) Hong, M.; Griffin, R. G. *J. Am. Chem. Soc.* **1998,** *120,* 7113−7114.
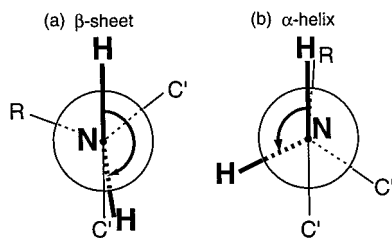(16) Michal, C. A.; Jelinski, L. W. *J. Am. Chem. Soc.* **1997,** *119,* 9059−9060.

Figure 1. Newman projection of a peptide residue showing the different ϕ_H torsion angles for the β-sheet (a) and the α-helical (b) conformation.

experiment yielded a simple 2D spectrum that showed exclusively the signals of the α-helical residues.[12]

In this paper, we demonstrate that a similar filtration approach can be used to identify β-sheet residues in proteins having high sensitivity and resolution. The nuclear spin interactions to be exploited for this purpose are the N−H and Cα−Hα dipolar couplings. The relative orientation between the N−H and Cα−Hα bonds reports on the ϕ torsion angle because $\phi_H = $ H−N−Cα−Hα is related to $\phi = $ C−N−Cα−C by $\phi_H = \phi - 60°$.[5] The ϕ_H angle is about $165°-180°$ in the extended β-sheet structure but about $-120°$ in the α-helical conformation (Figure 1).[19] The distinct geometries give rise to different dipolar evolution under the sum and difference of the two couplings. We show here that by choosing the time point corresponding to the largest difference, we can retain the β-sheet signals and remove the α-helical resonances. Similar to the α-helix filter, this β-sheet filter can be combined with a 2D correlation pulse sequence to better separate the resonances. In this way, we obtain a high-resolution β-sheet "fingerprint" of proteins without time-consuming 3D data acquisition. In the following text, we describe the experimental design and demonstrate it on a mixture of model amino acids and on selectively and extensively (S&E) ^{13}C-labeled[10,20] and uniformly ^{15}N-labeled ubiquitin.

Experimental Section

Sample Preparation. ^{15}N-labeled L-valine and ^{15}N−(*tert*-butoxy-carbonyl)-L-alanine (*N*-tBoc-Ala) were purchased from Cambridge Isotope Laboratory (Andover, MA). ^{15}N-acetyl-L-valine (NAV) was synthesized from L-valine according to published procedure,[22] except that the final drying was done using a Labconco freeze-dry system rather than treatment with benzene and dry ethyl acetate. The yield of the synthesis was 95%.

Selectively and extensively ^{13}C-labeled and uniformly ^{15}N-labeled ubiquitin was purchased from VLI−Research, Inc. (Malvern, PA). For the custom synthesis, cells were grown in M9 minimal media with [2-^{13}C] glycerol and ^{15}N-ammonium sulfate (Cambridge Isotope Laboratory, Andover, MA) as the sole carbon and nitrogen sources, respectively. As described before, in the S&E ^{13}C labeling scheme, specific carbons are enriched at high levels, while other sites are not labeled at all.[10,20] With [2-^{13}C] glycerol as the sole carbon precursor, ^{13}C spins are propagated into 18 out of 20 amino acids in the ^{13}Cα position. Nine of these Cα sites have no directly bonded ^{13}C neighbor; thus, isolated spins are created by this procedure. Approximately 25 mg of ubiquitin in powder form was packed into a rotor and then hydrated to 30 wt % H$_2$O. Ubiquitin was chosen for demonstrating
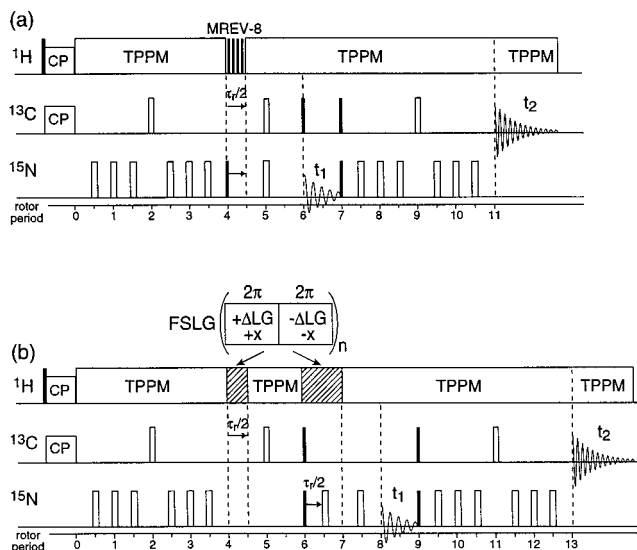

Figure 2. Pulse sequences for the β-sheet filter experiment: (a) the N−H nondoubled version is suitable for slow spinning speeds; (b) the N−H doubled version is suitable for higher spinning speeds. Filled and empty rectangles represent 90° and 180° pulses, respectively. HNCH dipolar evolution is active for one-half of a rotor period, $\tau_r/2$. Homonuclear ^{1}H−^{1}H decoupling is achieved by MREV-8 (a) and FSLG (b) sequences. CP, cross polarization; TPPM, two-pulse phase modulation.

this NMR technique because of its stability and its well-known three-dimensional structure.[21]

NMR Experiments. All NMR experiments were carried out on a Bruker DSX-400 spectrometer (Karlsruhe, Germany) operating at a resonance frequency of 100.72 MHz for ^{13}C, 400.49 MHz for ^{1}H, and 40.59 MHz for ^{15}N. The sample was placed in a 4-mm spinning module in a triple-resonance MAS probe. The ^{1}H radio frequency (rf) field strengths for homonuclear MREV-8 decoupling[23] and heteronuclear TPPM decoupling[24] were 100 kHz and 85 kHz, respectively. Carbon and nitrogen 90° pulse lengths were 4.0 μs and 5.6 μs, respectively. Cross-polarization contact time was 0.7 ms. A spinning speed of $\omega_r/2\pi = 4252$ Hz was chosen for the N−H nondoubled β-sheet filter experiment (Figure 2a). At this frequency, each rotor period accommodates seven MREV-8 cycles. The corresponding ^{1}H pulse length in the MREV-8 sequence was 2.8 μs. For the N−H doubled version of the experiment (Figure 2b), a spinning speed of $\omega_r/2\pi = 6600$ Hz was chosen and the frequency-switched Lee−Goldburg (FSLG) sequence was employed for homonuclear decoupling.[25,26] The FSLG decoupling field along the effective field was about 90 kHz. The spinning speeds were regulated to within $\pm$ 3 Hz by a Bruker MAS pneumatic control unit. For the indirect dimension, the evolution time was incremented by one rotor period until a maximum evolution time of 11 ms. A recycle delay of 2.5 s was used in all experiments. All measurements were carried out at room temperature ($T = 293 \pm 1$ K).

The frequency switching in the FSLG sequence was accomplished by modulating the phase of each 360° pulse in a linear and semi-continuous fashion.[27] The phase values were encoded in a shape file. Phase modulation and frequency modulation are equivalent because

$$\cos[(\omega_0 + \omega_{fslg})t + \phi] = \cos[\omega_0 t + (\phi + \omega_{fslg}t)] =$$
$$\cos[\omega_0 t + (\phi + \phi_{fslg})] \quad (1)$$

where ω_{fslg} is the frequency offset and ω_0 is the Larmor frequency. To

(17) Baldus, M.; Geurts, D. G.; Hediger, S.; Meier, B. H. *J. Magn. Reson. A* **1996**, *118*, 140−144.

(18) Sun, B. Q.; Rienstra, C. M.; Costa, P. R.; Herzfeld, J.; Williamson, J.; Griffin, R. G. *J. Am. Chem. Soc.* **1997**, *119*, 8540−8546.

(19) Creighton, T. E. *Proteins: Structures and Molecular Properties*, 2nd ed.; W. H. Freeman and Co.: New York, 1993.

(20) Hong, M.; Jakes, K. *J. Biomol. NMR* **1999**, *14*, 71−74.

(21) Vijay-Kumar, S.; Bugg, C. E.; Cook, W. J. *J. Mol. Biol.* **1987**, *194*, 531−544.

(22) Greenstein, J. P.; Milton, W. *Chemistry of the Amino Acids*; Wiley: New York, 1961.

(23) Rhim, W.-K.; Elleman, D. D.; Vaughan, R. W. *J. Chem. Phys.* **1973**, *58*, 1772−1773.

(24) Bennett, A. E.; Rienstra, C. M.; Auger, M.; Lakshmi, K. V.; Griffin, R. G. *J. Chem. Phys.* **1995**, *103*, 6951−6958.

(25) Bielecki, A.; Kolbert, A. C.; Levitt, M. H. *Chem. Phys. Lett.* **1989**, *155*, 341−346.

(26) Bielecki, A.; Kolbert, A. C.; de Groot, H. J. M.; Griffin, R. G.; Levitt, M. H. *Adv. Magn. Reson.* **1990**, *14*, 111−124.

satisfy the Lee−Goldburg condition, $\omega_{fslg}/\omega_{1,eff} = \cos (54.7°) = 1/\sqrt{3}$, where $\omega_{1,eff}$ is the strength of the effective field. The amplitude of the phase modulation for a 360° pulse is set to 208°, because

$$\frac{208°}{360°} = \frac{\phi_{fslg}}{\phi_{1,eff}} = \frac{\omega_{fslg}t}{\omega_{1,eff}t} = \cos(54.7°) \quad (2)$$

The phase-modulation method of achieving frequency switching has the advantage that it does not require any delays between consecutive 360° pulses, which is in contrast to direct frequency jumps using the Bruker hardware. In addition, the use of shaped pulses for FSLG considerably simplifies the programming of pulses on the heteronuclear channels.

The resonance assignment of the 2D ^{15}N−^{13}C spectra of ubiquitin was carried out on the basis of the liquid-state chemical shifts of ubiquitin,[28] and refined by solid-state NMR experiments that was shown recently. The secondary structure for each residue was assigned according to the X-ray crystal structure of ubiquitin.[21]

Simulation of Dipolar Modulation Curves. The time evolution under the sum and difference of the N−H and Cα−Hα dipolar couplings was simulated using a Fortran program that was described earlier.[8] The simulation was carried out for one rotor period according to eq 4. Effective dipolar coupling strengths for the C−H coupling tensor, the nondoubled N−H coupling tensor, and the doubled N−H tensor were calculated by multiplying the various dipolar coupling constants with the appropriate scaling factors for the multiple-pulse sequence used. The coupling constants are $\delta_{C−H} = 23.2$ kHz, $\delta_{N−H} = 11.1$ kHz, and $\delta_{N−Hx2} = 22.2$ kHz. The theoretical scaling factors κ for MREV-8 and FSLG are 0.471 and 0.577, respectively. Powder averaging was performed in 3° increments for all three Euler angles. Further input parameters were the spinning speed and the number of time-domain points. All simulations were performed on a Macintosh G4 computer requiring only a few minutes of computation time per simulation.

Pulse Sequences for the β-Sheet Filter. Two pulse sequences of the β-sheet filter experiment are shown in Figure 2. Version (a) is suitable for slow spinning speeds of about 5 kHz or less, while version (b) is preferred for faster spinning speeds of about 6−10 kHz. The former is carried out by probing the C−H and N−H dipolar couplings simultaneously, while the latter employs selective doubling of the N−H dipolar coupling to make the magnitudes of the C−H and N−H couplings comparable. This N−H doubling extends the spinning speed range of the experiment and enhances the angular resolution of the technique, as described previously.[29,30]

In both sequences, cross-polarization from ^{1}H to ^{13}C creates the ^{13}C magnetization. This magnetization then evolves under the ^{13}C−^{15}N dipolar interaction into antiphase coherence of the form C_yN_z, where C and N refer to ^{13}C and ^{15}N spins, respectively. The ^{15}N−^{13}C coupling is recoupled by a REDOR pulse train.[31,32] The subsequent evolution of the C_yN_z coherence differs for the two pulse sequences. In sequence (a), a ^{15}N 90° pulse converts the antiphase magnetization into zero- and double-quantum coherence C_xN_y. This evolves under the C−H and N−H dipolar couplings simultaneously for one-half of a rotor period, $\tau_r/2$. During this time, heteronuclear dipolar decoupling is replaced by ^{1}H−^{1}H homonuclear decoupling, which is achieved by an MREV-8 sequence. At the end of the rotor period, 180° pulses are applied on the ^{13}C and ^{15}N channels to refocus the isotropic chemical shift interaction. After a second rotor period, a 90° ^{13}C pulse converts the C_xN_y coherence into ^{15}N antiphase magnetization C_zN_y so that ^{15}N chemical-shift frequency can be encoded during the evolution period t_1. The evolved ^{15}N single-quantum coherence is converted back to

(27) Vinogradov, E.; Madhu, P. K.; Vega, S. *Chem. Phys. Lett.* **1999**, *314*, 443−450.
(28) Wang, A. C.; Bax, A. *J. Am. Chem. Soc.* **1996**, *118*, 2483−2494.
(29) Hong, M.; Gross, J. D.; Rienstra, C. M.; Griffin, R. G.; Kumashiro, K. K.; Schmidt-Rohr, K. *J. Magn. Reson.* **1997**, *129*, 85−92.
(30) Gullion, T.; Schaefer, J. In *Advances in Magn. Reson.*; Warren, W. S., Ed.; Academic Press: San Diego, 1989; Vol. 13, pp 57−83.
(31) Gullion, T.; Schaefer, J. *J. Magn. Reson.* **1989**, *81*, 196−200.
(32) Pan, Y.; Gullion, T.; Schaefer, J. *J. Magn. Reson.* **1990**, *90*, 330.
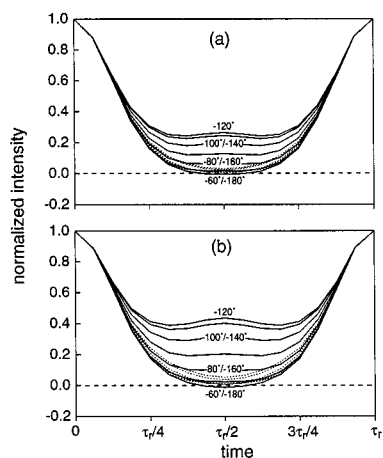
observable ^{13}C magnetization by a pair of 90° pulses and an identical REDOR period. Finally, ^{13}C isotropic chemical shift signal is acquired during t_2.

In the N−H doubled-pulse sequence (b), the spin coherence evolves under the C−H and N−H dipolar interactions separately but synchronously. First, the antiphase ^{13}C magnetization C_yN_z created by REDOR evolves under the C−H dipolar Hamiltonian for $\tau_r/2$. It is then converted to ^{15}N single-quantum coherence C_zN_y and evolves under the N−H dipolar coupling. Both the C−H and N−H dipolar evolution periods are established by ^{1}H−^{1}H decoupling through an FSLG sequence. While FSLG decoupling is applied for one-half a of rotor period for the C−H interaction, it is active for an entire rotor period for the N−H coupling. Combined with a ^{15}N 180° pulse in the middle of the N−H rotor period, the one-rotor-period FSLG decoupling doubles the dynamic phase of the N−H coupling. This is manifested as an apparent doubling of the N−H coupling strength.[29] Because the 180° pulse also recouples the ^{15}N chemical-shift anisotropy, a second ^{15}N 180° pulse in a second rotor period under heteronuclear decoupling is needed to refocus the CSA interaction. The rest of the pulse sequence is identical to the nondoubled experiment.

In both pulse sequences, the magnetization at the beginning of the t_1 period is reduced by the HNCH evolution. Therefore, the resonances in the resulting 2D spectra are attenuated by an amount that depends on the torsion angle, ϕ, of the specific residues. If desired, either pulse sequence can be converted into a real 3D experiment to precisely measure the torsion angles, ϕ. This would involve incrementing the HNCH period for one whole rotor period instead of using a constant evolution time of $\tau_r/2$. The resulting third dimension would exhibit characteristic dipolar sideband patterns corresponding to the torsion angle ϕ.

The average Hamiltonian during the $\tau_r/2$ HNCH dipolar modulation is

$$\hat{H}(\tau_r/2) = \kappa(\Psi_{CH}(\tau_r/2)2\hat{C}_z^{\alpha}\hat{H}_z^{\alpha} + \Psi_{NH}(\tau_r/2)2\hat{N}_z\hat{H}_z^{N}) \quad (3)$$

where κ is the scaling factor for the homonuclear decoupling sequence, and $\Psi_\lambda(\tau_r/2)$ ($\lambda =$ C−H, N−H) represents the MAS dynamic phases that are accumulated due to the N−H and C−H dipolar couplings. The dipolar interactions modulate the NMR signals according to

$$\cos\left[\frac{\Psi_{CH}(\tau_r/2) + \Psi_{NH}(\tau_r/2)}{2}\right] + \cos\left[\frac{\Psi_{CH}(\tau_r/2) - \Psi_{NH}(\tau_r/2)}{2}\right] \quad (4)$$

This amplitude modulation depends on the mutual orientation of the C−H and N−H tensors, which reports on the torsion angle ϕ_H. Thus, the intensities of the time-domain data can be simulated to yield the ϕ torsion angle, as shown before.[5]

Results and Discussion

Calculated HNCH Dipolar Modulation Curves. Figure 3 shows the simulated HNCH dipolar evolution curves for ϕ angles ranging from −180° to +180°. Two spinning speeds, $\omega_r/2\pi = 4252$ Hz (Figure 3a) and $\omega_r/2\pi = 6600$ Hz (Figure 3b), were considered. The simulations of the former assumed MREV-8 homonuclear decoupling, while those of the latter assumed FSLG homonuclear decoupling and the doubling of the N−H coupling. Each dipolar evolution curve corresponds to two ϕ torsion angles. Due to the uniaxiality of the dipolar interaction, the experiment does not distinguish between $+\phi_H$ angles and $-\phi_H$ angles. Because $\phi = \phi_H + 60°$, a double degeneracy exists for two ϕ angles related by $\phi_A + \phi_B = 120°$. For $\phi \in[-120°, -180°]$ and $\phi \in[-120°, -60°]$, the HNCH time signals are very sensitive to the ϕ angles. The residual intensities at the center of the rotor period $\tau_r/2$ range from the highest possible value, for $\phi = -120°$, to about 0. Simulations in this angular range were displayed at 10° ϕ-angle increments (solid lines). In contrast, in the remaining Ramachandran space of $\phi \in[-60°, 180°]$, the angular dependence of the HNCH

Figure 3. Simulated HNCH dipolar evolution curves as a function of the evolution time τ for various ϕ torsion angles. Curves are plotted at 10° increments for ϕ angles from −180° to −60° (solid lines) and at 20° increments for ϕ angles ranging from −60° to +180° (dotted lines). (a) With MREV-8 homonuclear decoupling, a spinning speed of 4252 Hz, and no N−H dipolar doubling. (b) With FSLG homonuclear decoupling, a spinning speed of 6600 Hz, and N−H dipolar doubling.
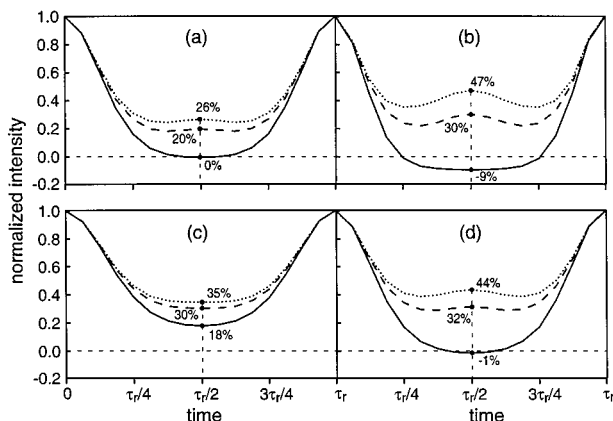

Figure 4. Selected ϕ-angle dependent HNCH dipolar evolution curves as a function of the evolution time τ. The intensities at the center of the rotor period are indicated. Only the curves for the ideal parallel β-sheet ($\phi = -120°$, dotted lines), antiparallel β-sheet ($\phi = -140°$, dashed lines), and α-helix ($\phi = -60°$, solid lines) are shown. (a) Without N−H doubling, with MREV-8 decoupling, and a spinning speed of 4252 Hz. (b) With N−H doubling, MREV-8 decoupling, and a spinning speed of 4252 Hz. (c) Without N−H doubling, with FSLG decoupling, and a spinning speed of 6600 Hz. (d) With N−H doubling, FSLG decoupling, and a spinning speed of 6600 Hz.

dipolar intensities is much smaller, with the $\tau_r/2$ intensities fluctuating between 0 and 0.1. For simplicity, the curves are displayed at 20° increments (dotted lines).

To represent the HNCH intensities at $\tau_r/2$ more clearly, we display the three curves corresponding to the ϕ angles for the classical parallel β-sheet (−120°), antiparallel β-sheet (−140°), and α-helix (−60°) conformations in Figure 4. In addition to varying the spinning speed, we also compare the N−H doubled experiment (panels b and d) with the nondoubled experiment (panels a and c) at each spinning speed. The α-helix and β-sheet conformations exhibit drastically different intensities at the center of the rotor period. At a spinning speed of 4252 Hz, without N−H doubling (a), the $\tau_r/2$ intensity of the classical β-sheet conformations is 26% − 20%, while the α-helical conformation exhibits vanishing intensities. Thus, fixing the HNCH evolution time to $\tau_r/2$ should filter out most of the helix signals. Incorporation of N−H doubling at the same spinning

speed (b) generates even larger differences between the helical and sheet structures. At $\tau_r/2$, the intensities of ideal parallel and antiparallel β-sheet conformations are 47% and 30%, respectively, while the α-helical residues exhibit a negative intensity of −9%. The increased angular resolution results from the fact that the doubled N−H coupling is comparable to the C−H coupling, so that the difference frequency in eq 4 approaches zero, which gives rise to a slow-decaying component in the time signal.

With complete resolution and sufficient sensitivity in the spectra, the negative and positive intensities for various ϕ torsion angles could be used to distinguish the various conformations. However, if the resonances are incompletely separated in the spectra, which is common for complex insoluble proteins, then the negative intensities of helical residues may well overlap with the positive intensities of sheet residues to cause partial cancellation of the intensities. Thus, the N−H doubled experiment under slow spinning speeds will not be readily useful for incompletely resolved spectra.

For solid-state NMR experiments of insoluble proteins, it is generally desirable to use higher spinning speeds to improve the spectral resolution. However, high spinning speeds compromise the performance of many multiple-pulse homonuclear decoupling sequences becasue as the cycle time of the decoupling sequence approaches the rotation period, the approximation of a constant average Hamiltonian during each decoupling cycle breaks down. This restriction is less severe for the FSLG sequence[25] due to its relatively short cycle time. For example, for a ¹H rf field strength of 100 kHz, the FSLG cycle time is 16.3 μs, but the corresponding cycle time for semi-windowless MREV-8 is 30 μs. Thus, FSLG is the preferred homonuclear decoupling sequence at higher spinning speeds.[33]

Figure 4c−d displays the HNCH dipolar evolution curves at a spinning speed of 6600 Hz, which was calculated using the FSLG scaling factor. The N−H nondoubled simulation (c) shows a much smaller difference between secondary structure elements as compared to the slow spinning case. The β-sheet signals at $\tau_r/2$ are 35% and 30% of the full intensity for the classical parallel and antiparallel β-sheet conformations, respectively, although the α-helical signals is only 18%. This reduced distinction is not surprising because faster spinning allows less time for anisotropic decay. Upon doubling of the N−H dipolar coupling, the removal of the helix intensities is considerably more complete: at $\tau_r/2$, the helix signals decay to −1% while the parallel and antiparallel β-sheet residues retain the intensities at 44% and 32%, respectively (Figure 4d).

These simulated HNCH dipolar evolution curves indicate that the β-sheet filter experiment should be implemented either under slow spinning without N−H doubling, or under fast spinning with N−H doubling. Although the former can be performed with most of the homonuclear decoupling sequences, the latter is preferably implemented with FSLG in order to avoid the interference between homonuclear decoupling and magic-angle spinning.

β-Sheet Filtered Spectra of Model Amino Acids. To demonstrate the utility of this simplified ϕ-angle technique for selecting the β-sheet signals, we tested the experiment on a mixture of two model amino acids, ¹⁵N-tBoc-Ala and ¹⁵N-acetyl-L-valine (NAV). The former has a ϕ torsion angle of −75.9°, which corresponds to the NMR ϕ_H angle of −135.9°,[34,35] but the latter has a ϕ angle of −136.5°, which is equivalent to

(33) vanRossum, B. J.; deGroot, C. P.; Ladizhansky, V.; Vega, S.; deGroot, H. J. M. *J. Am. Chem. Soc.* **2000**, *122*, 3465−3472.
(34) Meervelt, L. V.; Wael, K. D.; Zeegers-Huyskens, T. *J. Mol. Struct.* **1995**, *356*, 183−190.
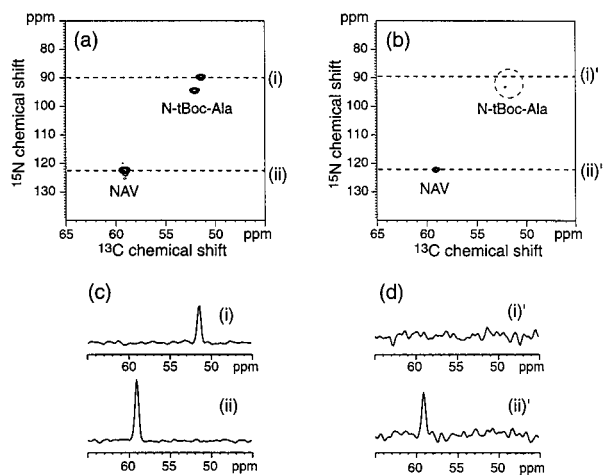
Figure 5. 2D β-sheet filtered spectra of a mixture of ^{15}N-acetyl-L-valine and ^{15}N-tBoc-L-alanine: (a) control and (b) β-sheet filtered and N–H doubled spectra, acquired under a spinning speed of 4252 Hz and with MREV-8 homonuclear decoupling. Cross-sections of the (c) control and (d) β-sheet filtered spectra indicate the degree of filtration. A total of 160 complex data points was acquired in F1 with 16 (a) and 32 (b) transients per t_1 increment, yielding acquisition times of approximately 2 and 4 h, respectively.

$\phi_{\mathrm{H}} = -163.5°$.[36] Thus, *N*-tBoc-Ala and NAV represent the helix and sheet conformations, respectively, and NAV is expected to be selectively detected by the current experiment.

The 2D β-sheet filtered spectra of ^{15}N-tBoc-Ala and ^{15}NAV are shown in Figure 5. To increase the angular resolution between the two ϕ angles, we performed a N–H doubled experiment at a spinning speed of 4252 Hz, using MREV-8 as the homonuclear decoupling sequence. Simulations (not shown) of the dipolar dephasing curves under these conditions show that the *N*-tBoc-Ala signal has vanishing intensity after an evolution time of one-half of a rotor period, although 36% intensity should be retained for NAV. Spectrum (a) represents the control measurement with TPPM decoupling of protons throughout the pulse sequence. This is equivalent to a conventional ^{15}N–^{13}C 2D HETCOR experiment. Two peaks are observed for *N*-tBoc-Ala, which most likely correspond to molecules in two different crystalline environments. The most downfield peak in the spectrum is assigned to NAV. In panel c, rows parallel to the ^{13}C dimension and taken from the NAV resonance and from one of the two N-tBoc-Ala resonances are shown.

The β-sheet filtered spectrum of the amino acid mixture is shown in Figure 5b, where the *N*-tBoc-Ala signals are sufficiently removed, but the NAV peak is retained. In panel d, rows of the same cross-sections as in c are plotted to illustrate the effect of α-helix signal suppression. It should be noted that the combination of slow spinning at 4252 Hz, N–H doubling, and MREV-8 homonuclear decoupling results in negative intensity for an ideal α-helix with $\phi \approx -60°$ (see Figure 4b). However, because *N*-tBoc-Ala deviates from the ideal α-helix structure, the current N–H doubled β-sheet filter experiment at slow spinning speed provides the most efficient β-sheet selection.

β-Sheet Filtered Spectra of Ubiquitin. The application of β-sheet filter experiments to proteins in the solid state was demonstrated on S&E ^{13}C-labeled and uniformly ^{15}N-labeled
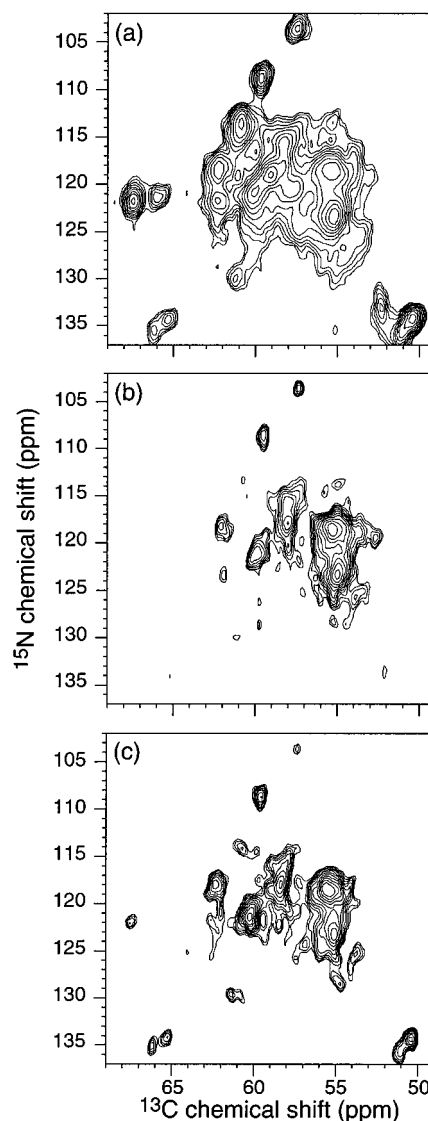
(35) Benedetti, E.; Blasio, B. D.; Pavone, V.; Pedone, C. *Biopolymers* **1981**, *20*, 1635−1649.

(36) Carroll, P. J.; Stewart, P. L.; Opella, S. J. *Acta Crystallogr.* **1990**, *C46*, 243−246.

Figure 6. 2D ^{15}N–^{13}C correlation spectra of ubiquitin: (a) without the β-sheet filter; spinning speed, 6600 Hz; 64 scans per t_1 increment; (b) N–H nondoubled β-sheet filter; spinning speed, 4252 Hz; 160 scans per t_1 increment; $\tau = \tau_r/2 = 117.6$ μs; and (c) N–H doubled β-sheet filter; spinning speed, 6600 Hz; 128 scans per t_1 increment; $\tau = \tau_r/2 = 75.8$ μs. Total acquisition times for spectra (a), (b), and (c) were 6.5, 11.5, and 14 h, respectively. Each spectrum was plotted with 12 contour levels, covering 4.5% to 100% of the maximal intensity.

ubiquitin.[10,20] Figure 6 displays three spectra, acquired without the β-sheet filter (a), with the N–H nondoubled β-sheet filter (b), and with the N–H doubled β-sheet filter (c). To compare these spectra fairly, we plotted each spectrum with the same minimum and maximum contour heights, at 4.5% and 100% of the maximal intensity, respectively.

Figure 6a displays the ^{15}N–^{13}C 2D spectrum of ubiquitin acquired without any β-sheet filtration. This was achieved using the pulse sequence of Figure 2b but replacing the homonuclear FSLG decoupling with heteronuclear TPPM decoupling. The spectrum serves as a reference in which all ^{13}Cα and ^{15}N spin pairs belonging to all conformations exhibit signals.[15,16] About a dozen resonances are resolved in the spectrum; the rest fall into a congested region at (^{15}N, ^{13}C) = (112 ppm−127 ppm, 53 ppm−63 ppm) where the contours are partially agglomerated. The limited line widths can be attributed to the finite ^{1}H decoupling field strength, rf inhomogeneity, and possible conformational heterogeneity in the sample.

The application of the β-sheet filter without N–H doubling considerably simplifies the 2D spectrum (Figure 6b), as intensities from residues with unfavorable geometries are attenuated by the HNCH dipolar modulation. Most notable is the nearly complete disappearance of the four proline α and δ resonances around (135 ppm, 66 ppm) and (135 ppm, 51 ppm), respectively. Similarly, a pair of signals at (122 ppm, 67.5 ppm) and (121 ppm, 66 ppm), which have been assigned to Val-26 and Ile-30,[10,28,37,38] are completely filtered from the spectrum. In addition, the β-sheet filter removed enough α-helix signals that the central congested region is now semi-resolved into three regions, with several resolved peaks at the periphery.

The N–H doubled β-sheet filter experiment at a spinning speed of 6600 Hz gave rise to a qualitatively similar spectrum (Figure 6c) as the nondoubled version. However, careful comparison reveals subtle differences between the two. Some resonances filtered out in the N–H nondoubled spectrum reappear with low intensities in the N–H doubled spectrum. These include the proline α and δ resonances and the V26 peak. The differences in the proline signals can be understood on the basis of the lack of the amide proton in prolines: because only the C–H dipolar coupling is present during the HNCH evolution period, no ϕ_H angle information is encoded for the prolines. Thus, the HNCH decay curves of the proline α and δ sites differ between the two experiments solely due to the spinning speeds. Numerical simulations of C–H dipolar decay indicate that the intensity at $\tau_r/2$ drops down to 8% at the spinning speed of 4252 Hz, but it is a nonnegligible 28% at the spinning speed of 6600 Hz (simulation not shown). Fortunately, the presence of the proline peaks in the spectrum does not complicate the β-sheet identification, because the proline resonances are readily identifiable on the basis of their large ^{15}N chemical shift[39] and the coexistence of the Cα and Cδ resonances within each ^{15}N cross-section.

The reappearance of the V26 resonance (122 ppm, 67.5 ppm) in the N–H doubled β-sheet filtered spectrum compared to the nondoubled spectrum is likely a result of the fast spinning and the high labeling level (100%) of the valine Cα site. We have observed that the valine signals in ubiquitin are exquisitely sensitive to spinning speeds, with higher intensities under faster spinning. This suggests that residual dipolar coupling between Cα and Cβ, both of which are labeled at 100% by the [2-^{13}C] glycerol precursor,[10] contribute to line broadening. A similar mechanism may also account for the increased intensities of V70 (130 ppm, 61 ppm), F45 (124 ppm, 57 ppm), S57 (114 ppm, 61 ppm), and T14 (121 ppm, 62 ppm) in the N–H doubled β-sheet filtered spectrum.

On the other hand, several peaks that are present in the N–H nondoubled β-sheet filtered spectrum (Figure 6b) are attenuated in the N–H doubled correspondent (Figure 6c). These include E34 (114 ppm, 55 ppm), E18 (119.5 ppm, 53 ppm), and I13 (129 ppm, 60 ppm). Because these amino acid residues are synthesized from the citric acid cycle, their ^{13}C-labeling levels are 50% or lower.[10] Thus, the intensity differences between the two spectra may be partially attributed to insufficient sensitivity. Other possible reasons will be discussed below.

In addition to the spectra shown here, we have also acquired an N–H nondoubled β-sheet filtered spectrum at a spinning speed of 6600 Hz using FSLG decoupling (not shown). The spectrum resembles the unfiltered, reference spectrum to a large
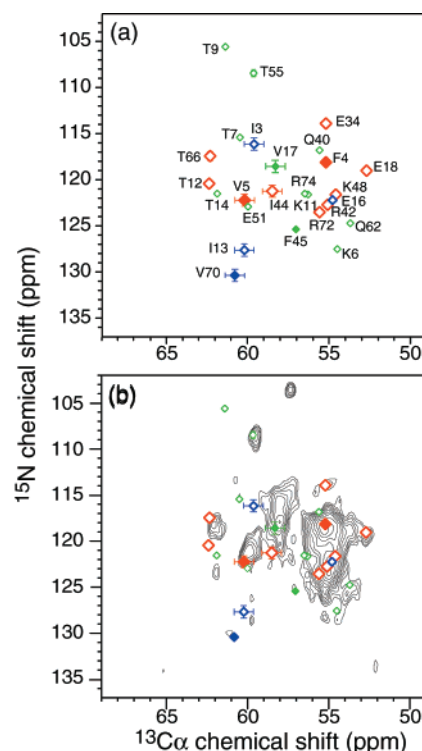
(37) Hong, M. *J. Biomol. NMR* **1999**, *15*, 1–14.
(38) Hong, M. *J. Magn. Reson.* **1999**, *136*, 86–91.
(39) Wishart, D. S.; Sykes, B. D.; Richards, F. M. *J. Mol. Biol.* **1991**, *222*, 311–333.

Figure 7. Comparison between (a) the expected β-sheet spectrum of ubiquitin according to its crystal structure and (b) the experimental β-sheet spectrum, acquired without N–H doubling. Large red diamonds: $\phi = -120° \pm 5°$. Medium blue diamonds: $\phi = -110° \pm 5°$. Small green diamonds: $\phi = -100° \pm 5°$. Filled symbols: residues with 100% Cα labeling. Open symbols: residues with 50% or lower Cα labeling.

degree, which confirms the reduced contrast between the helix and the sheet intensities under these conditions (see Figure 4c).

Comparison with Solution NMR and X-ray Data. To assess the selectivity and accuracy of the β-sheet filter technique, we compared the experimental β-sheet filtered spectra to the anticipated β-sheet resonance positions based on the crystal structure of ubiquitin.[21] The simulated spectrum is displayed in Figure 7a. The ^{15}N and ^{13}C frequencies were primarily taken from the solution NMR chemical shifts[28] but were refined by solid-state NMR values for those that have been resolved and assigned previously.[10,37,38] The uncertainty in the solid-state NMR values due to the digital resolution of the 2D and 3D spectra is represented by error bars.

Because the various ϕ-angles in the β-sheet conformational region give rise to slightly different dipolar decay curves, we bracketed the peak intensities into three categories according to the ϕ angles obtained from the crystal structure: the strongest intensities are expected for $\phi = -120° \pm 5°$ (large red symbols), medium intensities for $\phi = -110° \pm 5°$ (medium blue symbols), and weak intensities for $\phi = -100° \pm 5°$ (small green symbols). Further contributing to the intensity differences are the varying ^{13}C-labeling levels inherent to the S&E ^{13}C-labeling protocol.[10] Filled symbols represent residues with high ^{13}C-labeling levels (100%), and open signals denote sites with low ^{13}C-labeling levels (50% or less).

Figure 7b shows the superposition of the simulated β-sheet pattern with the experimental N–H nondoubled β-sheet spectrum (also Figure 6b). As expected, the strongest signals result from the highly labeled residues F4 and V5, both of which possess a ϕ torsion angle close to $-120°$. A medium signal is expected for V70 because its ϕ angle is approximately $-110°$,

but the observed intensity at (130 ppm, 61 ppm) is relatively weak. However, the intensity is increased in the fast-spinning spectrum (Figure 6c), which suggests that slow spinning attenuated the peak intensity in the nondoubled spectrum. Two highly labeled residues with torsion angles around −100° are V17 and F45. The former accounts for a strong signal at (118.5 ppm, 58 ppm), while the latter exhibits a weak signal at (124 ppm, 57 ppm). Again, this F45 signal is boosted when the spinning speed is increased to 6600 Hz (Figure 6c).

Other resonances in the spectrum can be assigned to residues with lower ^{13}C-labeling levels (open symbols), which are synthesized by the citric acid cycle. Among the residues with ϕ angles of around −120° (red open diamonds), T66 and T12 account for one strong unresolved peak centered at (118.5 ppm, 62 ppm), and I44 is poorly resolved from the strong V17 resonance. Glutamic acid residues E34 and E18 have torsion angles of approximately −120° in the crystal structure and exhibit well-resolved peaks. Finally, an unresolved group of peaks around (123 ppm, 55 ppm) are assigned to R72, R42, and K48.

The two glutamic acid residues, E34 and E18, do not manifest intensities above the minimum contour level in the N−H doubled β-sheet spectrum (Figure 6c). This may be partly attributed to the difference between the crystal and the solution NMR structures of the protein. The solution NMR structure indicates that both residues have ϕ torsion angles of approximately −110°, rather than −120°.[28] If this held true for the solid sample, then the intensities of these residues would be reduced. In addition, because N−H dipolar doubling enhances the distinction between various torsion angles even within the β-sheet manifold (Figure 2), the intensity difference for $\phi = $ −120° to $\phi = $ −110° is larger in the N−H doubled experiment than in the nondoubled correspondent. This mechanism would further discriminate against the E34 and E18 signals.

Three resonances belong to the category of β-sheet residues having low ^{13}C-labeling levels and with a torsion angle of about −110° (open blue diamonds). These are I3 and I13, which show weak signals, and E16, which contributes to the cluster of peaks at (123 ppm, 55 ppm). The remaining low-intensity signals in the spectrum can be assigned to weakly labeled amino acid residues with torsion angles around −100° (open green diamonds). These include R74, K11, Q40, Q62, and K6. Residue T7 is not detected in the slow-spinning spectrum but is manifested clearly in the N−H doubled, fast-spinning, spectrum (Figure 6c).

When comparing the solid-state β-sheet spectrum with the solution chemical shifts, we find small chemical-shift changes for residues I13, I3, T7, and V70. Differences between the solution and the solid-state chemical shifts have been previously documented in the literature[40−42] and may be attributed to packing effects. Finally, no resonance in the β-sheet filtered spectrum matches the solution chemical shifts of T9, which has a ϕ torsion angle of −100°. However, this is not an imperfection of the β-sheet filter experiment because no intensity is observed at the solution T9 frequencies, even in the unfiltered 2D ^{15}N−^{13}C spectrum. Thus, the T9 peak has shifted significantly for reasons that are presently unknown. Low labeling levels can

(40) Ye, C.; Fu, R.; Hu, J.; Hou, L.; Ding, S. *Magn. Reson. Chem.* **1993**, *31*, 699−704.

(41) Straus, S. K.; Bremi, T.; Ernst, R. R. *J. Biomol. NMR* **1998**, *12*, 39−50.

(42) McDermott, A. E.; Polenova, T.; Bockmann, A.; Zilm, K. W.; Paulsen, E. K.; Martin, R. W.; Montelione, G. T. *J. Biomol. NMR* **2000**, *16*, 209−219.

be ruled out as a contributing factor because several other threonine residues such as T55 exhibit strong signals. The difference may have a structural origin, because the solution ^{15}N chemical shift of this residue is more upfield than all other threonine residues in ubiquitin.

Comparison to the α-Helix Filter. It is instructive to compare the β-sheet filtered spectra to the complementary α-helix filtered spectrum of the same protein shown recently (Figure 6b in[12]). Clear differences can be seen for residues V70 and K6, which exhibit intensities in the β-sheet spectrum but are completely suppressed in the α-helix spectrum. In contrast, V26 and S57 residues show strong resonances in the α-helix spectrum but have nearly vanishing signals in the β-sheet spectra. Another example is the peak cluster (^{15}N, 117−125 ppm; ^{13}C, 56 ppm), which is largely attenuated in the α-helix spectrum but is strong in the β-sheet spectrum. This is consistent with the notion that this spectral region is rich in β-sheet resonances. Therefore, the combined use of the two filter techniques enhances the confidence and accuracy of structure determination. In addition, subtle differences between the two β-sheet spectra may be understood by referring to the α-helix spectrum. For example, the V26 resonance is filtered out in the N−H nondoubled β-sheet spectrum but exhibits nonnegligible intensity in the N−H doubled spectrum. However, even the residual signal is weak relative to the corresponding signal in the α-helix spectrum; thus, one can confidently identify V26 to be α-helical.

Application of the β-Sheet Filter to Uniformly Labeled Peptides and Proteins. The β-sheet filter experiment described here relies on the selection of the Cα resonances directly bonded to the amide nitrogen by a ^{15}N−^{13}C dipolar coherence filter. We have demonstrated this successfully on ^{13}C-unlabeled amino acids and on S&E ^{13}C-labeled proteins. The experiment should also be largely applicable to uniformly ^{13}C-abeled peptides and proteins. The influence of other ^{13}C sites near Cα, namely ^{13}CO and ^{13}Cβ, can be suppressed by the use of short ^{1}H−^{13}C CP contact times and short ^{15}N−^{13}C REDOR mixing times, respectively. The residual effect of ^{13}C−^{13}C dipolar couplings, which may be introduced via rotational resonance, is minor. The only relevant undesirable coherences are those that generate Cα signals through one-bond couplings from CO or Cβ coherence that is present during the N−H and C−H interaction period. These coherence terms are scaled by powder averages of sine-modulated factors such as $\langle \sin(\omega_{CO-N}\tau)\sin(\omega_{CO-C\alpha}\tau) \sin(\omega_{C\alpha-N}\tau)\rangle$, where τ is the length of the REDOR excitation and reconversion periods. Because these sinusoidal terms can be of either sign, the powder averages are generally small. Therefore, signal contributions from these multi-spin coherences should be negligible. In fact, the strongest effect of rotational resonance, if unavoidable, is not so much these secondary couplings but the line-broadening it induces.

Conclusion

We have demonstrated an efficient high-resolution solid-state NMR method for identifying the β-sheet residues in solid proteins. On the basis of the different mutual orientations of the N−H and Cα−Hα tensors between α-helices and β-sheets, distinct HNCH dipolar modulation trajectories result. We have shown on model amino acids that it is sufficient to record signal intensities at the center of the dipolar evolution period, where the α-helix and β-sheet intensities differ most, without sampling the dipolar modulation at many time points. This constant-time dipolar modulation can be combined with 2D ^{15}N−^{13}C heteronuclear correlation to filter out the helix signals and retain the

sheet signals with good site resolution. We have applied this technique to S&E ^{13}C-labeled ubiquitin. The experimental *β*-sheet filtered spectrum shows good agreement with the anticipated *β*-sheet pattern of ubiquitin, thus confirming the utility of this method for identifying *β*-sheet residues with site resolution. Pulse sequences suitable for both high and low spinning speeds are demonstrated and compared.

The 2D *β*-sheet filter experiment is more efficient than 3D torsion-angle experiments and is applicable to multiply labeled proteins. It represents a complementary approach to the recently introduced α-helix filter experiment, which selects the α-helix signals and destroys the *β*-sheet signals according to the magnitudes of the Cα chemical-shift anisotropy. We anticipate that the combined use of these two pattern-recognition-based techniques will facilitate and considerably increase the accuracy of protein structure determination in the solid state.